



Study of wet and dry etching processes for antimonide-based photonic ICs

SHAMSUL ARAFIN,^{1,2,*} ANTHONY P. MCFADDEN,³ BANAFUL PAUL,² SYED M. N. HASAN,² JAMES A. GUPTA,⁴ CHRIS J. PALMSTRØM,^{1,3} AND LARRY A. COLDREN^{1,3}

¹Department of Electrical and Computer Engineering, University of California at Santa Barbara, Santa Barbara, CA, USA

²Department of Electrical and Computer Engineering, The Ohio State University, Columbus, OH, USA

³Department of Materials, University of California at Santa Barbara, Santa Barbara, CA, USA

⁴National Research Council of Canada, Ottawa, ON, Canada

*arafin.1@osu.edu

Abstract: We report on the dry etch process parameters and the associated etch rates for target and mask materials, as well as surface roughness in an inductively coupled plasma (ICP) for the (AlGaIn)(AsSb)-compounds. The essential chemistry is based on Cl₂ with the addition of N₂ for sidewall passivation. The optimized ICP etch process is capable of producing high aspect ratio structures with smooth sidewalls. *In situ* reflectance monitoring with a 670-nm-wavelength laser was used to enable stop-etching at a material interface with high accuracy. Given the additional need for highly selective wet chemical etchants in the fabrication of GaSb based electronic and optoelectronic devices, an extensive investigation was also performed to examine numerous etch solutions. These etchants were listed with etch rates, selectivities, and surface roughness in order to validate their suitability for intended applications. Despite the frequent use of GaSb or InAsSb materials for etch stop layers against each other, devices where their unique type-II broken bandgap alignment is undesired require new selective wet etchants between GaSb and AlGaAsSb with good selectivity. All of the wet chemical and dry etching processes described here were optimized using an *n*-type GaSb substrate.

© 2019 Optical Society of America under the terms of the [OSA Open Access Publishing Agreement](#)

1. Introduction

Dry and wet etch processes are important and widely used for the fabrication of electronic and optoelectronic devices. Recently, there has been an increasing interest in many micro and nanoscale short-wave (SW-) and mid-wave (MW) infrared (IR) devices including transistors [1,2], photodiodes [3], light emitting diodes (LEDs) [4] and diode lasers [5] due to a wide range of emerging applications. Development of these devices at this wavelength regime requires the novel (AlGaIn)(AsSb) material system on GaSb substrates.

As opposed to III-Vs such as phosphides and arsenides, antimonide materials exhibit a few unusual etching behaviors such as undesired weak etching by commonly used developers with an etch rate of up to 0.6 nm/sec and very fast oxidation rate with atmospheric oxygen. It is also observed that hydrofluoric acid (HF) etches plasma-exposed antimonides unlike other III-Vs. Moreover, GaSb and its alloys show poor selectivities in commonly used wet and dry etchants that are typical in other III-V's device processing. Due to the strong and fast oxidation, Al-containing materials are not useable as etch-stop layers [6].

As a standard practice, for fabricating many optoelectronic devices including widely-tunable lasers, e.g. sampled-grating distributed-Bragg-reflector (SG-DBR) [7] and vertical-cavity surface-emitting lasers (VCSELs) [8], one usually uses etch-stop layers in order to control the etch depth with high accuracy of nanometer order. In such a way, it is possible to selectively remove the desired materials against another layer. In the case of widely-tunable

lasers, leading to photonic ICs (PICs) where active and passive regions are defined by selective wet chemical etching, multi-quantum well (MQW) regions are selectively removed from the top of the waveguide layer, defining low-loss passive waveguides [9]. This is usually done by the wet etch with an etch stop layer, since the wet etch makes no intrinsic damage in the laser structure. Not only this, a good wet etch process is also needed to create smooth surfaces and to etch to the correct depth to prevent exposure of the Al-containing layers, which would make regrowth difficult because of the difficulty in removing Al_2O_3 . Therefore, developing viable etch processes to make PIC compatible widely-tunable lasers in the GaSb-based materials, is of utmost importance.

For antimonide-based SG-DBR lasers, one has to find a good etch-stop layer underneath the MQW region. A lattice-matched InAsSb or InAs layer could be a good choice [10]. However, insertion of such a thin layer of InAsSb under the MQW region introduces a type-II band alignment in the structure, prohibiting a good flow of carriers into the well. Therefore, developing a dry etch process is extremely important so that the etch can be stopped on a material change using an optical etch-stop monitor, which uses the different index or bandgap properties of the stopping layer rather than its chemical properties.

Despite the fact that dry etching performed by ionized gases is almost always anisotropic and leaves smooth surfaces, it always creates some damages (leading to non-radiative recombination centers) on the etched surface and its underlying layers to a certain depth [11]. Having an understanding on the damage depth leads us to calculate the ionization energy. In this work, we used an inductively-coupled-plasma (ICP) reactive-ion-etching (RIE) which can produce a high density of reactive etching species at relatively low ion energy for low damage.

For the GaSb-based PICs, a surface-ridge waveguide will be required to connect the lasers, amplifiers, modulators and other photonic components together monolithically. The surface-ridge waveguide has a good current confinement, low-loss for single mode waveguides, which makes it uniquely suitable for lasers [12]. In GaSb-based PICs, quaternary AlGaAsSb with 50% or higher aluminium compositions could be used as a top cladding layer. In order to make a low-loss surface ridge waveguide, it is extremely important to find and optimize a dry etching recipe. The optimization of the process is focused on the sidewall verticality, surface smoothness and flat bottom in the etched profile.

There are a few studies that report only wet etch processes for antimonide materials [10,13–15]. However, the etchant lists presented in these studies are not complete because of the lack of information on a few useful wet and dry etchants and their suitability, etch stop layers except InAsSb against GaSb and etching of quaternary alloys. As a result, developing robust processes for widely tunable lasers and PICs by relying on these studies will not be possible, requiring a more systematic and thorough study.

Despite of the frequent use of lattice-matched InAsSb as an etch stop layer, its use in SG-DBR laser is not appropriate due to the type-II band alignment with GaSb. This forces to explore alternative etch-stop materials. In this paper, we performed detailed study not only on several unreported but useful wet etchants but also on dry etching with real-time, *in situ* laser etch depth monitoring and the corresponding etch results are summarized. In fact, our etching efforts were extended from binary to quaternary and even quaternaries alloys, their etching rates, selectivities as well as usability. Finally, the GaSb substrate removal process is described. The comprehensive detailing on the selective dry and wet etching for antimonides and its alloys will be beneficial for the fabrication of next-generation high-quality optoelectronic and electronic devices.

2. Experimental procedure

2.1 Sample preparation

To study and develop the dry and wet etch processes, we used four different samples with epistacks on GaSb:Te substrates grown by molecular beam epitaxy. Figure 1 shows the

schematic of the epilayers of the etching test structure used in this dry and wet etching study. The samples with Al-containing layers were covered with a 8-10 nm GaSb cap layer to prevent oxidation.

Standard photolithography was used to define the arbitrary patterns in the photoresist. In all of the wet etching tests, photoresist as etch masks were used. In cases of dry etching, especially when surface-ridge waveguides were defined, a 100-nm layer of SiO₂ is deposited via plasma-enhanced chemical vapor deposition on the as-grown sample at first. The lithographically-defined arbitrary patterns were then transferred to the SiO₂ by a CF₄/CHF₃/O₂ ICP-RIE etch. Finally, the photoresist was removed by the appropriate solvents in an ultrasonic bath. The target antimonide materials were then etched with SiO₂ as an etch mask. Note that the etch depth of the target materials was measured using a Dektak profilometer.

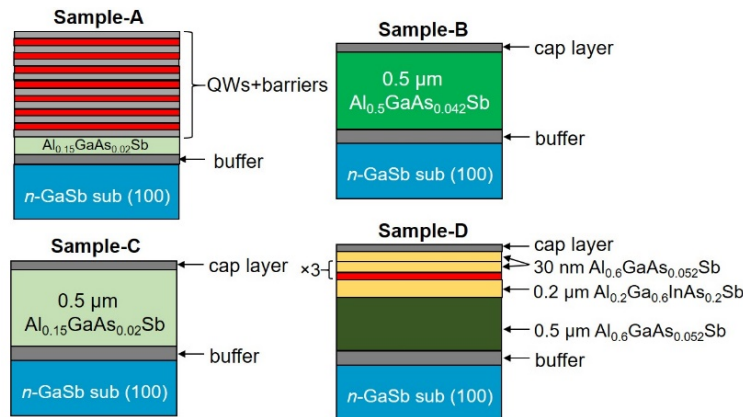


Fig. 1. Schematics of different test samples with epilayers used in this dry and wet etching study.

While processing InP-based lasers, the surface-ridge waveguide needs to be aligned to the $\langle 011 \rangle$ crystal direction of InP, because the top InP cladding etch is normally finished with an HCl-based crystallographic wet etch [16]. It is extremely important to investigate whether a similar behavior is applicable for the GaSb-based material system. Considering this, a mask was designed with narrow stripes at different angles. Figure 2 shows the microscope images of the 5 μm wide patterns obtained after photolithography using image reversal photoresists on a 100 nm blanket SiO₂ layer.

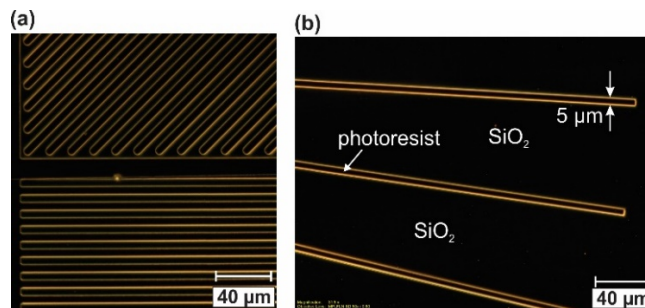


Fig. 2. Microscope images of the test samples with 5- μm surface ridges obtained after development and ready for dry etching in order to transfer the patterns into the hard mask.

Surface-ridge profiles obtained in this study involved first applying the Ti/Au metal stack over the entire epi-surface, and then performing a lithographic step to protect the metal where ridges were desired, followed by an etch step to remove the metal layers everywhere except

on the ridge tops to be. The photoresist/Ti/Au was then used as a mask for the ridge etching with Cl_2/N_2 chemistry using ICP-RIE.

2.2 Preparation of etch solutions

The preparation methods used in this wet etching study is different from the techniques described in ref [10]. The “Transene’s” premix solutions were often used in order to obtain consistent etch results. Such premixes are also easier to deal with since one does not need to mix up solid crystals with water every time prior to etching. Some of the premixes used in this study were as follows:

1. The tartaric acid-based premix is called “Rochelle” etch solution. This is 15 g of $\text{C}_4\text{H}_4\text{KNaO}_6$ crystals, dissolved in 200 ml of DI- H_2O , similar to ref [10]. In order to perform etching using this premix, one has to just add HCl and H_2O_2 to match the solution [10].
2. The citric acid premix, similar to mentioned in ref [10], is also used and it is better than mixing a supersaturated solution.
3. Sirtl etch is a mixture of HF and CrO_3 in DI water. This premix was also used in this study at two different dilutions, i.e., 1:5 = Sirtl: H_2O and 1:100 = Sirtl: H_2O .

2.3 Etch reactor with etch depth monitor

A Cl_2/N_2 ICP-RIE was used for dry etching performed in this study. The ICP has a laser monitor installed for getting real-time data during etching. Using this *in situ* etch monitoring system, one can observe the oscillation fringes, primarily between the surface and the first interface, and stop the etch exactly at the point needed. Later the etch rate and etch depth in real time enabling control of process termination were calculated using the 670 nm visible laser. Therefore, it is important to have the reliable material data. i.e.; refractive index and extinction coefficient for the material of interest at this wavelength. Based on the simulations of laser reflectance from a proposed sample, the etching process can be controlled to provide an endpoint depth precision within ± 10 nm.

3. Etching results and discussion

3.1 Dry etching

The etch parameters, and the associated etch results including etch-rate and etch-mask selectivity are listed in Table 1.

Table 1. ICP Dry Etching Parameter* and the Corresponding Results for Sample-B

RF bias (W)	ICP (W)	Pressure (Pa)	Gas flow (sccm)		Etch rate (nm/sec)	Selectivity vs SiO_2
			Cl_2	N_2		
75	900	0.2	20	10	8.7	8

*ICP plasma etching was performed using the Panasonic E640 system that is not capable of displaying induced self-DC bias voltage during the etching process and therefore it is not mentioned.

Although we have not obtained an accurate number for the ionization energy in our ICP system, the low RF chamber bias of 75 W suggests that it is relatively low. Importantly, by the addition of nitrogen to the etching RF plasma, our etch process resulted in smooth and less damaged surface. The presence of N_2 gas flow during the etching process helps to reduce the surface roughness and consequently smooth surface could be obtained. In addition, we did

not use argon in the gas chemistry in order to avoid physical etching. Therefore, the developed etch recipe based on Cl_2/N_2 is expected to work for even high Al content layers with good surface morphology. In fact, one of the major attributes of ICP is supposed to be the low ion damage imparted to the surface. Given the fact that the sample will be subsequently annealed in the MBE chamber prior to regrowth, we do not expect this damage to be an issue. Moreover, in a DBR laser, the etching is never over the MQW active region, so we did not pursue this matter further.

In order to obtain the etch rate, the etching was performed on etching test sample-B for three different times. After the dry etching, a smooth surface morphology on the etched surface was observed. Quaternary lattice-matched $\text{Al}_{0.5}\text{GaAs}_{0.04}\text{Sb}$ cladding layer was the layer of interest in this case. The measured data is fitted with the transfer matrix method in order to extract the refractive index and extinction coefficient values of the quaternary cladding layer. The reflectivity of a thin-film stack was continuously calculated as the stack was progressively thinned by etching from one side. Finally, the reflectivity vs. etch depth plot is used to determine end-points during etching.

Figure 3 shows the measured reflectivity data vs etch depth of the etching test structure. The intensity of the oscillations in the reflectivity data gradually increases as the material is being etched more; hinting that there is less absorption of light within the material of interest. The discontinuity at the end of the 500 nm lattice-matched $\text{Al}_{0.5}\text{GaAs}_{0.04}\text{Sb}$ layer is due to the transition to GaSb, and the slight mismatch may be due to the imaginary part being incorrect. The discontinuity seems to occur right at the layer transition according to the fits. So by eye, one can see the termination of each layer in the laser monitor plot itself, and one should be able to clearly see the first dip with lower extinction than the AlGaAsSb dips, and start counting from this point.

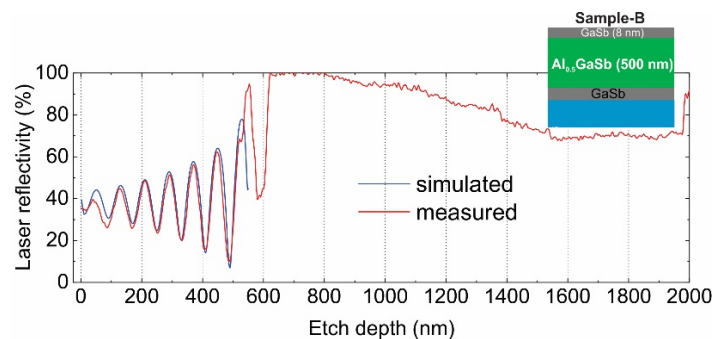


Fig. 3. Measured reflectivity data vs etch depth of etching test structure-B. Simulated laser monitor signal is superimposed to extract the refractive index and extinction coefficient values of the quaternary cladding layer.

Ridge processing was ended with a clean-up wet-etch to remove damage at the etched surface and the sidewalls. In other words, after the first waveguide dry etch, the surface ridge waveguide was then etched by an HCl-based isotropic wet etch. Figure 4 shows the ridge waveguide with a vertical etch profile and smooth surface morphology after clean-up etching. Rough sidewall, mostly due to a wavy SiO_2 mask edge defined by contact lithography, and possibly also enhanced by defects in epilayers, can also be seen here. In spite of the ridge-edge roughness in the waveguide, this is not a concern since a better lithography with a stepper should solve this issue. Although no undercut of mask was observed for dry etching, some undercut for the HCl wet etching was observed, which does selectively attack the AlGaAsSb epilayer. Most importantly, no crystallographic etching was observed for various orientations. A porous sidewall was noticed in the sample which could be attributed to the defects in epilayers. The defects revealed after the clean-up etch were not a surprise as there was some lattice mismatch in this AlGaAsSb epilayer. Figures 4(c) and 4(d) present the SEM

images of 50 μm wide ridges obtained after performing ICP etching using resist/Ti/Au as an etch mask. As may be noted, one of the potential drawbacks is the side-wall roughness that results from a replication of the roughness of the combined photoresist/etched-gold mask into the semiconductor.

Figure 5(b) shows simulated and measured (smoothed) reflectivity data vs etch depth of test sample-A with MQWs. There is general agreement. The test sample was patterned with a 1 mm \times 1 mm region unmasked so that it could be etched to remove the MQW (passive). Figure 5(c) shows the original measured reflectivity data vs etch depth of the etching test structure. There are two humps in the profile. As soon as the 2nd dip is observed, it starts to rise, and finally gets flat, the etch needs to be stopped, indicating that the waveguide layer is reached. Figure 5(d) shows a microscope image of this test structure after etching, showing the active (unetched since covered with photoresist) and passive (etched) regions.

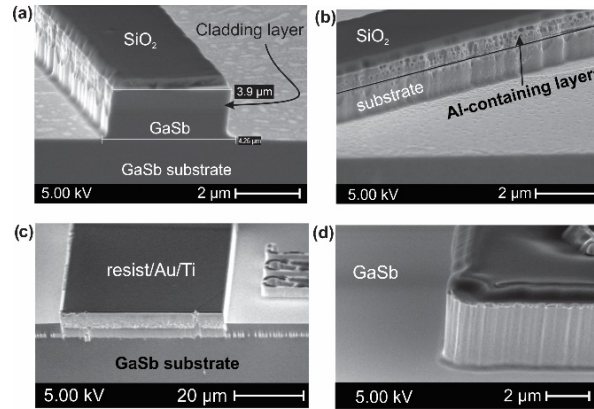


Fig. 4. SEM images of the test samples with 5- μm surface ridges obtained after (a) Cl_2/N_2 dry etching, (b) dry etching followed by 5 sec cleanup etching by HCl. Sidewalls can also be seen here after, (c) 50- μm wide stripes covered with resist and Ti//Au metal layer underneath after dry etching in Cl_2/N_2 plasma and (d) the close-up view of the ridges are shown at the bottom.

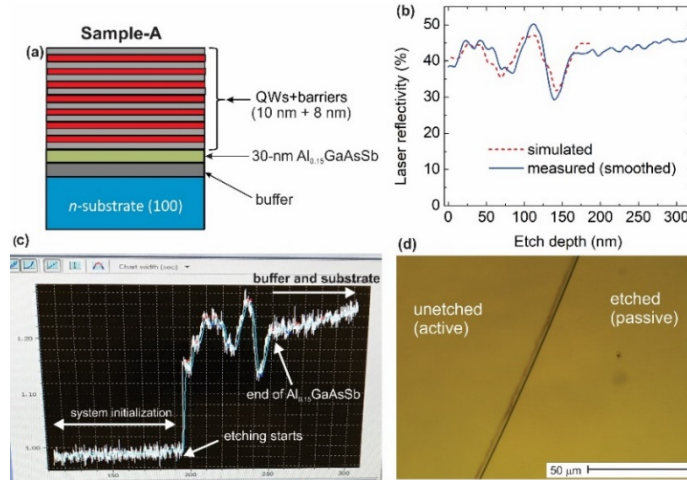


Fig. 5. (a) Schematic of the test structures for active/passive definition test, (b) simulated and measured (smoothed out) reflectivity data as a function of etch depth are superimposed; (c) system's original raw data for the detection of endpoint during dry etching using Cl_2/N_2 plasma; and (d) microscope image of the test structure after the etching, showing active/passive regions.

In order to assess the effect of the developed plasma etch process on our material structure, Fabry P rot broad-area lasers with a wide ridge using this ICP dry etch were fabricated. *I-V* characteristics of the device were then measured under both forward and reverse biases. Laser devices exhibit reasonable dark current and threshold current at room temperature, hinting that the plasma etch did not affect the device performance.

3.2 Wet chemical etching

A number of etchants along with the etch rates for different materials are listed in Table 2. One of the most-used wet etchants is Solution-1. Using this etchant, GaSb, InAs, and InGaAsSb are etched with a smooth surface and a good reproducibility. For Al-containing layers, this etchant shows fast etching rate when the Al-content is low (Al<30%). For the Solution-2, we found the same etch rates as reported by Dier *et al.* [10]. Most importantly, selective removal of InAsSb from GaSb can be done by this solution.

Table 2. Wet-Etchants for Antimonide Materials Used in This Study

#	Wet etchants	Etching rate (nm/sec)				
		GaSb	In _{0.43} GaAsSb	Al _{0.5} GaAs _{0.04} Sb	InAs _{0.91} Sb	Al _{0.2} In _{0.2} GaAs _{0.19} Sb
1	C ₄ H ₄ KNaO ₆ :HCl:H ₂ O ₂ = 50 : 40 : 3.5	12	6	5	0.4	4
2	C ₆ H ₈ O ₇ :H ₂ O ₂ = 2 : 1	0.01	0.23	-	1.5	-
3	HCl:H ₂ O ₂ :H ₂ O = 100 : 1 : 100	4.2	-	10	0.8	1
4	H ₃ PO ₄ : H ₂ O ₂ : C ₆ H ₈ O ₇ : H ₂ O = 3 : 5 : 55 : 22	2.5-3 (fairly unselective)				
5	AZ726 MIF developer	0.17 (GaSb/InAs superlattice)				
6	Buffered HF	570 (plasma exposed GaSb, AlGaAsSb and InAs)				

HCl-based etchant (Solution-3) could also be used in removing antimonide materials. However, the surface morphology of GaSb and low-Al containing materials usually gets rough with this etchant. Figure 6 presents the microscope image of the Al_{0.5}GaAsSb surface after being etched by this etchant, showing the surface roughness is about 8 nm, as measured by the surface profilometer. However, this etchant is useful because it shows good selectivity between lattice-matched quinary AlGaInAsSb and AlGaAsSb with 80% Al-composition. In fact, one could obtain a selectivity higher than 30 between the Al_{0.85}GaAs_{0.07}Sb and Al_{0.2}In_{0.25}GaAs_{0.23}Sb layer with a reproducible etch rate and smooth surface after the etching [17]. The etching rate for the etch stop layer is accurate and reproducible. The HCl etchant shows fast etching rate for Al-rich (Al>50%) layers. This high degree of selectivity confirmed that the Al_{0.2}In_{0.25}GaAs_{0.23}Sb alloy could be suitable for the etch stop layer [17].

Solution-4 can be used to etch antimonides with a moderate etching rate in an unselective way. It could be used for processing interband cascade laser [18] devices where several hundred to over a thousand epilayers of short-period antimonide-based superlattice with different constituents are grown as a part of the device structure. Solution-5 and 6 are not that useful as etchants. However, the device manufacturers should be aware of these two etchants as well as their etch rates.

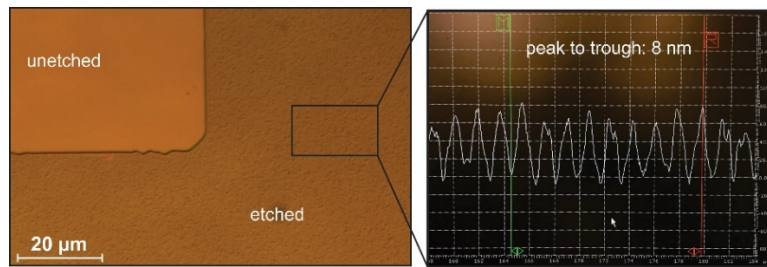


Fig. 6. Optical microscope image of the etched surface after wet chemical etching (left) of $\text{Al}_{0.5}\text{GaAsSb}$ by HCl-based etchant. Roughness measurement of the etched surface is also shown by the profilometer (right).

3.3 GaSb substrate removal

The substrate removal procedure is described in detail in ref [19]. This could be done by the SIRTl etchant which is referred to the mixture of HF/CrO_3 . Transene Inc. stocks two premixes, 1:5 and 1:10 Sirtl: H_2O . The former solution shows a very high etch rate of GaSb material, which one could begin with to remove the bulk of the material. Given that, this etchant exhibits very high selectivity between GaSb and InAsSb, 1:100 Sirtl: H_2O could be used to stop etching on thin layers of InAsSb. Thus, a smooth, mirror-like light-blue colored thin InAsSb layer can be obtained at the end of the removal process.

4. Conclusion

Selective wet and dry etching processes have been explored for the quaternaries lattice-matched to GaSb. Useful wet etchants and dry etching processes are given. In particular, materials and processes relevant to establishing a fabrication procedure for widely-tunable SG-DBR lasers in the SW/MW-IR wavelength regime using antimonide materials system have been defined. By employing an MQW InGaAsSb/AlGaAsSb/GaSb gain material and necessary processing steps, one could develop a PIC technology in the GaSb material system that contains a MQW active region, which is selectively removed either by a wet or dry etch using an etch stop layer or by a time-controlled etch, aided by a laser monitor if done by dry ion-etching. This makes the integration platform the simplest way to combine active and passive components on a chip. In fact, the fabrication of many other optoelectronic devices could benefit from the etching and processing technology outlined in this paper.

Acknowledgments

The authors gratefully acknowledge the help of Dr. Demis John for *in situ* dry etching of antimonides.

References

1. B. R. Bennett, R. Magno, J. B. Boos, W. Kruppa, and M. G. Ancona, "Antimonide-based compound semiconductors for electronic devices: A review," *Solid-State Electron.* **49**(12), 1875–1895 (2005).
2. M. Mohapatra, A. Mumtaz, and A. K. Panda, "Performance evaluation of GaSb/AlGaAs based high electron mobility transistors," in 3rd International Conference on Advances in Recent Technologies in Communication and Computing (ARTCom), Bangalore, India, 2011, pp. 249 – 252.
3. R. Chao, J. Wun, Y. Wang, Y. Chen, J. E. Bowers, and J. Shi, "High-speed and high-power GaSb based photodiode for 2.5 μm wavelength operations," in IEEE Photonics Conference (IPC), Waikoloa, HI 2016, pp. 472–473.
4. S. Suchalkin, S. Jung, G. Kipshidze, L. Shterengas, T. Hosoda, D. Westerfeld, D. Snyder, and G. Belenky, "GaSb based light emitting diodes with strained InGaAsSb type I quantum well active regions," *Appl. Phys. Lett.* **93**(8), 081107 (2008).
5. K. Kashani-Shirazi, K. Vizbaras, A. Bachmann, S. Arafin, and M.-C. Amann, "Low-threshold strained quantum-well GaSb-based lasers emitting in the 2.5- to 2.7- μm wavelength range," *IEEE Photonics Technol. Lett.* **21**(16), 1106–1108 (2009).
6. O. Blum, M. J. Hafich, J. F. Klem, K. Baucom, and A. Allennan, "Wet thermal oxidation of AlAsSb against As/Sb ratio," *Electron. Lett.* **33**(12), 1097–1099 (1997).

7. S. Arafin, A. P. McFadden, M. Pendharkar, C. J. Palmström, and L. A. Coldren, "Recent progress on GaSb-based photonic integrated circuits," in 14th International Conference on Mid-Infrared Optoelectronics, (MIOMD), Flagstaff, AZ, USA, 2018, pp. 1–2.
8. S. Arafin, A. Bachmann, K. Kashani-Shirazi, and M.-C. Amann, "Electrically-pumped continuous-wave vertical-cavity surface-emitting lasers at 2.6 μm ," *Appl. Phys. Lett.* **95**(13), 131120 (2009).
9. J. W. Raring, M. N. Sysak, A. Tauke-Pedretti, M. Dummer, E. J. Skogen, J. S. Barton, S. P. DenBaars, and L. A. Coldren, "Advanced integration schemes for high-functionality/high-performance photonic integrated circuits," in *SPIE* **6126**, 61260H (2006).
10. O. Dier, C. Lin, M. Grau, and M.-C. Amann, "Selective and non-selective wet-chemical etchants for GaSb-based materials," *Semicond. Sci. Technol.* **19**(11), 1250–1253 (2004).
11. S. J. Pearton, F. Ren, T. R. Fullowan, A. Katz, W. S. Hobson, U. K. Chakrabarti, and C. R. Abernathy, "Plasma etching of III–V semiconductor thin films," *Mater. Chem. Phys.* **32**(3), 215–234 (1992).
12. L. A. Coldren, S. C. Nicholes, L. Johansson, S. Ristic, R. S. Guzzon, E. J. Norberg, and U. Krishnamachari, "High Performance InP-Based Photonic ICs—A Tutorial," *J. Lightwave Technol.* **29**(4), 554–570 (2011).
13. X. Zhang, Y. Li, X. Wang, Y. Li, G. Yue, Z. Wang, J. Xie, J. Zhang, and Y. Hao, "Study on etch process of GaSb-based VCSEL," *Guangdian Gongcheng* **44**(12), 1225–1229 (2017).
14. M. You, Q. Sun, S. Li, L. Yin, X. Li, and J. Liu, "Study on HCl system wet-etching process of GaSb-based materials," in 4th International Conference on Machinery, Materials and Information Technology Applications, Atlantis Press, 2016.
15. H. Hong-Yue, X. Wei, W. Guo-Wei, X. Ying-Qiang, R. Zheng-Wei, H. Xi, H. Zhen-Hong, L. Yong-Ping, W. Si-Hang, and N. Zhi-Chuan, "Wet chemical etching of antimonide-Based infrared materials," *Chin. Phys. Lett.* **32**(10), 107302 (2015).
16. L. W. Stulz and L. A. Coldren, "Orientation of (100) InGaAsP/InP wafers by HCl chemical etching," *J. Electrochem. Soc.* **130**(7), 1628–1630 (1983).
17. S. Jung, "Mid infrared III-V semiconductor emitters and detectors," PhD dissertation, Stony Brook University, New York, USA, (2012).
18. S. M. S. Rassel, L. Li, Y. Li, R. Yang, J. Gupta, X. Wu, and G. Aers, "High-temperature and low-threshold interband cascade lasers at wavelengths longer than 6 μm ," *Opt. Eng.* **57**(1), 011021 (2018).
19. S. Arafin, "Electrically-pumped GaSb-based vertical-cavity surface-emitting lasers," PhD dissertation, Technical University of Munich, Munich, Germany, (2012).